Applied Physics Letters

Strain lithography for two-dimensional materials by electron irradiation

Cite as: Appl. Phys. Lett. **120**, 093104 (2022); https://doi.org/10.1063/5.0082556
Submitted: 16 December 2021 • Accepted: 21 February 2022 • Published Online: 03 March 2022

Shuo Du, Yang Guo, Xin Huang, et al.

© 2022 Author(s).

AIP Publishing

Strain lithography for two-dimensional materials by electron irradiation

Cite as: Appl. Phys. Lett. **120**, 093104 (2022); doi: 10.1063/5.0082556
Submitted: 16 December 2021 · Accepted: 21 February 2022 ·
Published Online: 3 March 2022

View Online

Export Citation

CrossMark

Shuo Du,[1,2] Yang Guo,[1,2,a)] Xin Huang,[1,2] Chi Sun,[1,2] Zhaoqian Zhang,[3] Leyong Hu,[1,2] Ruixuan Zheng,[1,2] Qinghu Bai,[1,2] Aizi Jin,[1] Haifang Yang,[1] Yanfeng Zhang,[3] Junjie Li,[1,4,a)] and Changzhi Gu[1,2,a)]

AFFILIATIONS

[1]Beijing National Laboratory for Condensed Matter Physics, Institute of Physics, Chinese Academy of Sciences, Beijing 100190, People's Republic of China
[2]School of Physical Sciences, CAS Key Laboratory of Vacuum Physics, University of Chinese Academy of Sciences, Beijing 100190, People's Republic of China
[3]School of Materials Science and Engineering, Peking University, Beijing 100871, People's Republic of China
[4]Songshan Lake Materials Laboratory, Dongguan 523808, People's Republic of China

[a)]Authors to whom correspondence should be addressed: yangguo@iphy.ac.cn; jjli@iphy.ac.cn; and czgu@iphy.ac.cn

ABSTRACT

Strain engineering, aiming to tune physical properties of semiconductors, provides a promising paradigm for modern micro/nanoelectronics. Two-dimensional materials (2DMs) are the ideal candidates for the next generation of strain engineered devices because of their intrinsic exceptional mechanical flexibility and strength. However, conventional strain modulation methods in 2DMs cannot satisfy the demand of future device applications, because strained structures by these methods lack consistency, reproducibility, and design flexibility. Here, based on the photoresist degeneration induced by electron irradiation, we present a non-contact approach to accurately and directly write the strains with designed patterns from the nanometer to micrometer scale in 2DMs. Profit from controllable manipulation of the electron beam, the developed strategy offers a capability for constructing tensile, compress, or complex strains in $MoSe_2$ monolayers; hence, unique electronic structures for unique physical properties can be designed. Aside from 2DMs, this approach is also appropriate for other types of materials such as Au, α-Si, and Al_2O_3. Its flexibility and IC-compatibility allow our strain lithography methodology promising in accelerating the potential applications of 2DMs in extensive fields ranging from nanoelectromechanical systems, high-performance sensing, and nontraditional photovoltaics to quantum information science.

Published under an exclusive license by AIP Publishing. https://doi.org/10.1063/5.0082556

Since Bardeen and Shockley's original work[1] on deformation potential of semiconductors in 1950, strain engineering has played a key role in modern microelectronics due to its strong ability to design material properties and device performance. For instance, strained silicon has been adopted in nearly all 90, 65, and 45 nm process nodes in the state-of-the-art CMOS devices.[2,3] However, in recent years, two-dimensional materials (2DMs) have presented greater advantages than conventional bulk semiconductors for developing new strain engineering technology in the fields ranging from high-performance sensing and nontraditional photovoltaics to quantum information science,[4] because they exhibit a large deformation tolerance[5] up to 10% and unique material properties such as strong excitonic effects,[6] chirality optical selection rules,[7] the free degree of pseudospin,[8] and spin-valley locking.[9]

Strain engineering of 2DMs has been mediated by modulations of diverse physical properties including electrical, magnetic, and optical properties in the recent decade.[10–16] Pseudo-magnetic fields higher than 300 T in graphene nanobubbles have been theoretically predicted and experimentally observed in the former studies.[15] Through nanoscale strain engineering with thin films and ferroelectrics, transition metal dichalcogenide (TMDC) $MoTe_2$ can be reversibly switched with electric-field-induced strain from a semi-metallic phase to a semiconducting phase in the field effect transistor geometry. The optical bandgap of a TMDC MoS_2 monolayer is able to be significantly tuned up to several hundred meV with ultra-large strains.[17,18] Piezotronic and piezo-phototronic effects in strained TMDCs have also been attracting growing attention in recent years with their applications involving strain sensors, nanogenerators, micro-/nanoelectromechanical systems, and photodetectors.[19–22] In addition, recent studies have

demonstrated quantum light emitters in atomically thin TMDC WSe_2 layers with strain induced quantum-dot-like potential wells for efficient funneling of excitons toward isolated quantum emitters, which are characterized by strong single photon anti-bunching signatures and zero-phonon exciton linewidths down to tens of μeV.[23–26]

Based on these achievements of strain engineering in 2DMs, it is the immediate requirement to precisely fabricate strained structures by tuning physical properties for the next application of large-scale integrated chips. Unlike strained silicon, however, the strained structures of 2DMs usually are built by extrinsic mechanical ways, for instance, bulging or folding by heating,[27,28] tenting with nanoparticles on substrates,[17,29–32] bending with flexible supporter,[33,34] etc.[11,35,36] Within the collection of these fabricating methods, few ones are plausible for consistency and repeatability of strained structures due to unguided self-organization processes. While some direct patterning approaches, such as thermomechanical nanopatterning,[37] possess good uniformity and flexibility in strain construction, the non-contact method that does not introduce contamination is still worth exploring. On the other hand, it would be a promising strategy to learn from nanolithographic techniques such as laser directly writing and electron beam exposure for building nano-strained structures,[38,39] which have been widely used for precise and programmable micro/nanofabrication of semiconductor devices.

Following this idea, here, we present a method for direct and precise generation of strained structures in 2DMs via electron irradiation by an electron beam lithography (EBL) system based on the effect of photoresist degeneration during injecting electrons into a polymethylmethacrylate (PMMA) layer. With EBL's graphical function of nanomanufacturing, we are able to precisely pattern tensile or compressive strains in 2DMs with controlled positions, shapes, and sizes tunable from the nanometer to micrometer scale. For instance, the strains of three bowl-shaped $MoSe_2$ monolayers with the same radius can be precisely modulated from 0.04% to 0.15% by using the dose from 50 to 150 As/cm^2; the maximal PL peak shift of a Mexican hat-shaped strain reaching about 64 meV is observed, corresponding to ~2.1% strain. In addition, we demonstrate that this method of strain lithography is also suitable for ultrathin films of other materials such Au, α-Si, and Al_2O_3. The universality of materials, flexiblity in complex strain construction, and compatibility with IC manufacture would enable our method to accelerate the potential applications of 2DMs in the extensive fields ranging from nanoelectromechanical systems, high-performance sensing, and nontraditional photovoltaics to quantum information science.

The schematic of controllably patterning strain in 2DMs via electron irradiation is illustrated in Fig. 1(a). A monolayer of $MoSe_2$ grown by the chemical vapor deposition (CVD) system is transferred onto the top of a spin-coated 600 nm PMMA (950 A7) layer, which serves as an electrosensitive deformable material. By controlling the sacnning path of the electron beam in the EBL system (Raith 150), the strain with the designed pattern will be constructed in $MoSe_2$ monolayers (detailed in Fig. S1 of the supplementary material).

Impacted by electrons, the $MoSe_2$ monolayer and the underlying PMMA are locally deformed as shown in Fig. 1(b) from steps 1 to 2. The electrons can easily penetrate the ultrathin $MoSe_2$ layer and have little effect on its lattice with appropriate doses.[40] However, when the electrons come to the PMMA layer, the impacted molecular strands of PMMA are easier to be broken, which cause the decrease in the local PMMA volume (detailed in Sec. II of the supplementary material).[41–44] During the deformation process of PMMA, the $MoSe_2$ layer stays physically intact and remains in conformal contact with PMMA through van der Waals interactions, forming a plastic deformation. The degree of deformation can be modulated to a certain extent by increasing the dose of the electron beam, as shown in step 3 of Fig. 1(b). To illustrate this process, three different levels of dot-type strains are prepared in a $MoSe_2$ monolayer, and their topography images of an atomic force microscope (AFM) are shown in Fig. 1(c). The dot-type patterns are exposed by the dot-exposure mode of EBL with the accelerating voltage of 10 kV. By increasing the dose from 2 to 8 pAs, the depth of strain dots increases from 37

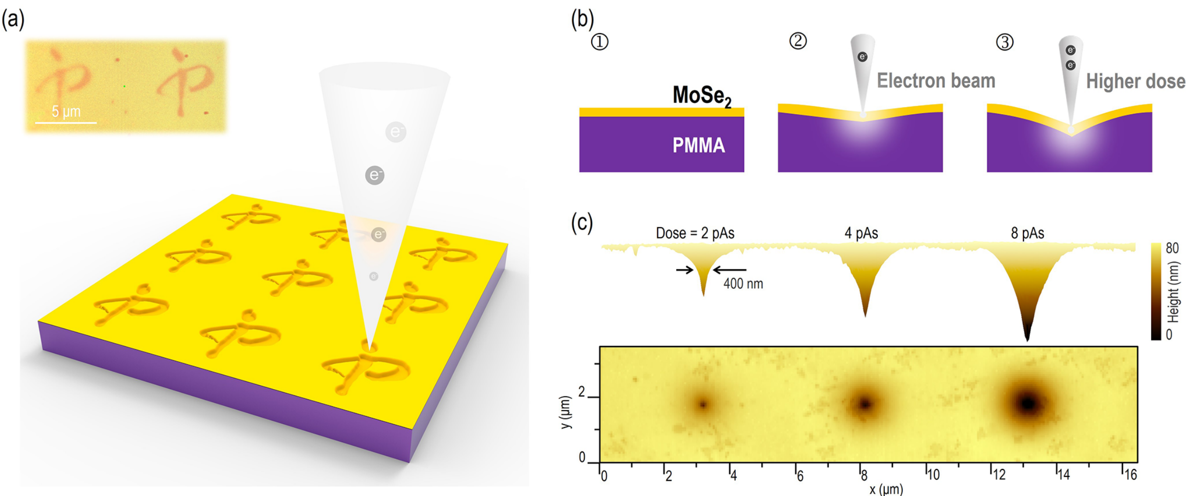

FIG. 1. Patterned strain imprinting via an electron beam in 2DMs. (a) Schematic of strain direct writing by using a focused electron beam on a $MoSe_2$ monolayer covering on a PMMA layer. The inset image is the optical image of the strained pattern (logo of institute of physics) in the $MoSe_2$ monolayer. (b) Process of strain evolution in a $MoSe_2$ monolayer with increasing electron dose. (c) AFM topography images of the strained dots in a $MoSe_2$ monolayer by injecting dose from 2 to 8 pAs.

Published under an exclusive license by AIP Publishing

to 80 nm, and the feature size (full width at half maximum, FWHM) varies from 400 to 800 nm.

As a fast and nondestructive technique, Raman spectroscopy is a powerful diagnostic tool to investigate the strain effects of 2DMs.[45–49] We performed Raman spectroscopy on $MoSe_2$ monolayers to characterize the deformation in the strained structures. For comparison, three circle-shaped strains in a $MoSe_2$ monolayer imprinted by an area-exposure mode of EBL (the difference between dot- and area-exposure modes of EBL is discussed in the Sec. III of the supplementary material) are fabricated. It can be seen from the AFM images in Fig. 2(a) that all strained $MoSe_2$ monolayers exhibit similar bowl-shaped features, and the depth increases from 5 to 15 nm with the dose varying from 50 to 150 μAs/cm^2 while the $MoSe_2$ bowl mouth keeps the same diameter. The calculated strain distributions of corresponding deformation profiles in Fig. 2(a) are shown in Fig. 2(b) via a finite-element method (FEM, detailed in Sec. I of the supplementary material), and the measured spatial distribution of the Raman peaks of A_1' (the out of plane mode) along with 2ZA (the double resonance of the acoustic mode)[48,49] of the $MoSe_2$ monolayer is presented in Figs. 2(c) and 2(d), respectively. It is obvious that both A_1' and 2ZA modes become softening in the exposure ranges with increasing the electron dose. Compared with the Raman bands of an unstrained $MoSe_2$ [Fig. 2(e)], the average Raman shifts of the A_1' mode in the $MoSe_2$ bowls are -0.3, -0.6, and $-1.1\,\text{cm}^{-1}$ for the corresponding electron dose of 50, 100, and 150 μAs/cm^2, respectively. According to the theoretical calculation reported before,[48] the biaxial strain induced A_1' mode's Raman-shift ratio is $-7.0\,\text{cm}^{-1}$ per % strain in the small strain range. So the average strains of three bowl-shaped $MoSe_2$ monolayers can be estimated as 0.04%, 0.09%, and 0.15%, respectively, which are close to the simulation results [Fig. 2(b)].

On the other hand, it is worthwhile to discuss whether the Raman-shifts observed in the strained structures include the electron bombardment effect, which would give spectral signatures that mimic strain. According to previous theoretical and experimental studies, irradiation with a high-energy ($\geq$60 keV) or high-density electron beam (electron number $> 1 \times 10^3\,\text{nm}^{-2} = 1.6 \times 10^4\,\mu\text{As/cm}^2$) could cause partial removal of selenium and correlate the dependence of the Raman peak shifts with selenium vacancy density.[50,51] However, the accelerating bias voltage of an electron beam used in our study is 10 kV (electron energy = 10 keV), and obviously, the electron density used here is about two orders smaller than this threshold value to induce chemical changes in materials. To experimentally exclude the electron bombardment effect in our samples, a set of $MoSe_2$ monolayers irradiated with the electron dose ranging from 10^2 to 10^4 μAs/cm^2 have been examined by Raman measurements (see Fig. S3 in the supplementary material). It can be found that the Raman-shifts of $MoSe_2$ monolayers below 400 μAs/cm^2 are quite small, indicating a negligible or weak electron bombardment effect. In addition, the Raman-shift mapping images shown in Fig. S3 present an inhomogeneous distribution in the range from 800 to 1200 μAs/cm^2, which could be attributed to generation and diffusion of selenium vacancies induced by injecting high-density electrons.[51]

This controllable strain generation method offers the flexibility for complex strain distribution (including tensile and compress strains) generation in 2DMs, which can be designed for a desired spatial profile of materials' electronic structures in any specific sites, presenting unique physical properties. To demonstrate this point, we prepared a strained $MoSe_2$ monolayer with a Mexican hat-shaped pattern (exposed by the electron beam in an annular area with the dose of 400 μAs/cm^2) and measured the strain-induced spatial bandgap profile of the $MoSe_2$ Mexican hat by using scanning photoluminescence (PL) spectroscopy. Figure 3(a) displays the PL peak position mapping image, and Figs. 3(b) and 3(c) are the peak position profile and a set of PL spectra of the cross section along the dashed line in Fig. 3(a), respectively. It is obvious that the PL peak exhibits a red-shift along the radial direction from the edge to center on the bottom of the $MoSe_2$ Mexican hat, while it turns back with a blue-shift on its hat tip. Such an energy profile corresponds to a Mexican hat-type electronic structure, as shown in Fig. 3(f). The maximal PL peak shift of about 64 meV is observed, which corresponds to ~2.1% strain, calculated by using the energy tuning ratio of 30 meV per % reported in the previous experimental studies.[48,52,53] It should be noted that the area of electron exposure is only located along the bottom of the $MoSe_2$ Mexican hat but not the central portion. So the blue shift of PL peaks in the central range would be originated from the edge effect of electron exposure, where the lattice expansion in the exposure range propagates to the central undisturbed region and induces a compressive strain in there. The contour profile of the region with PL peak shift matches with that of physical deformation shown in Figs. 3(e) and 3(f).

Furthermore, to illustrate the repeatability and uniformity of our method, an array of Mexican hat-shaped patterns is fabricated in a $MoSe_2$ monolayer, where the standard deviation of PL peak positions in the exposure area of these Mexican hat deformations is only 0.53 meV (detailed in Sec. V of the supplementary material). To further illustrate our approach's capability for complex electronic structures construction, various strained patterns (including triangle, spiral, chiral, etc.) are imprinted on $MoSe_2$ monolayers (shown in Sec. VI of the supplementary material), and the PL spectroscopic mapping images of a logo (insititute of physics) shaped strain in a $MoSe_2$ monolayer are also shown in Sec. VII of the supplementary material.

Figure 4(a) is a set of groove shaped strains on a $MoSe_2$ monolayer by the electron beam illuminating in a set of strip areas with each 10 nm wide. The height profile of the $MoSe_2$ nano-grooves and the amplified AFM topography image of one nano-groove are shown in Fig. 4(b). Compared with the unstrained area, the depth of the groove bottom is near 32 nm, and the height of each groove is near 10 nm with the FWHM about 90 nm. To identify the strain with nanoscale resolution below the optical diffraction limit, we performed an AFM-based tip-enhanced photoluminescence spectroscopy (AFM-TEPL) investigation over the groove shaped 2DMs,[54,55] as illustrated in Fig. 4(c) (detailed in Sec. I of the supplementary material). Figure 4(d) shows the scanning TEPL spectroscopic map plotting peaks of the strained $MoSe_2$ monolayer of the same groove in the white dashed area of Figs. 4(a) and 4(b), with pixel sizes 80 × 8.3 nm. Compared with the pixels in groove's edge, the peak position of the pixels in the groove moves about 1–4 meV with the width of 10–11 pixels (nearly 90 nm), which proves our method possesses the capability for differential strain distribution construction in the nanoscale. Compared with previous direct strain patterning methods for 2DMs (Sec. VIII of the supplementary material, Table S1), our non-contact strain patterning method is comparable and competitive in reducing pollutions (from the objects providing pressures), nanoscale resolution, and controllability of strain distribution.

Published under an exclusive license by AIP Publishing

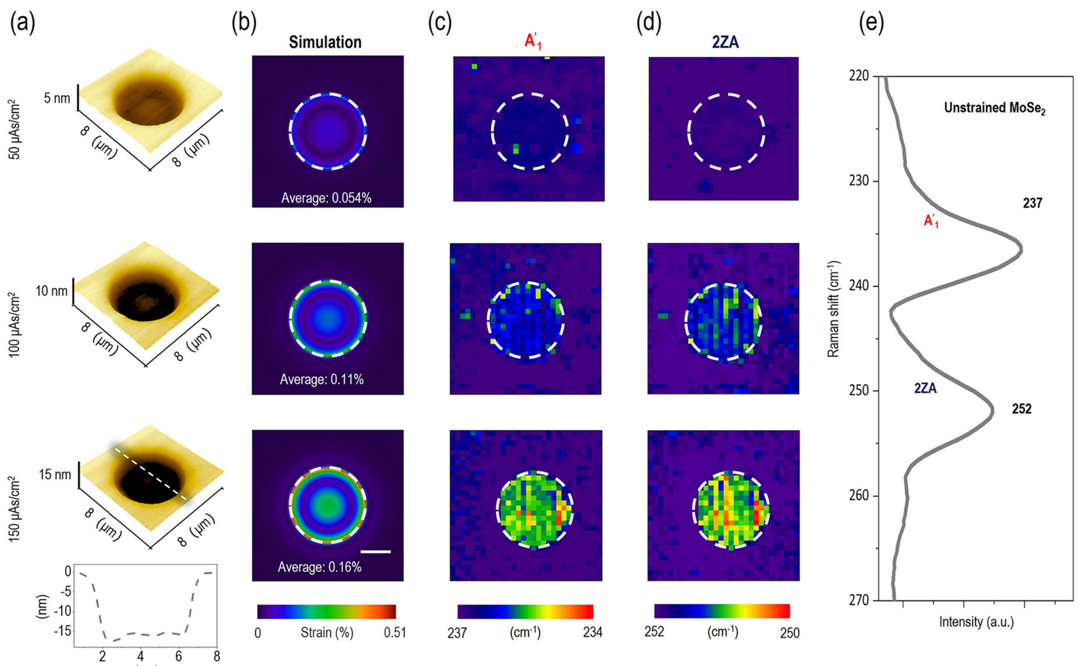

FIG. 2. Strain modulation on a $MoSe_2$ monolayer. (a) AFM images of strained bowl-shaped patterns in $MoSe_2$ monolayers with different electron doses of 50, 100, and 150 μAs/cm^2. The cross-sectional AFM image vertically cut along the white dashed line in the case of 150 μAs/cm^2 is shown in the bottom. (b) Simulated strain distributions of bowl-shaped deformations in $MoSe_2$ monolayers obtained by finite elements calculations. The scale bar is 1 μm. (c) and (d) Raman peak mapping images of three $MoSe_2$ strained patterns constructed with A'_1 (c) and 2ZA modes (d), where one pixel is 400 nm. (e) The Raman spectrum of an unstrained $MoSe_2$ monolayer.

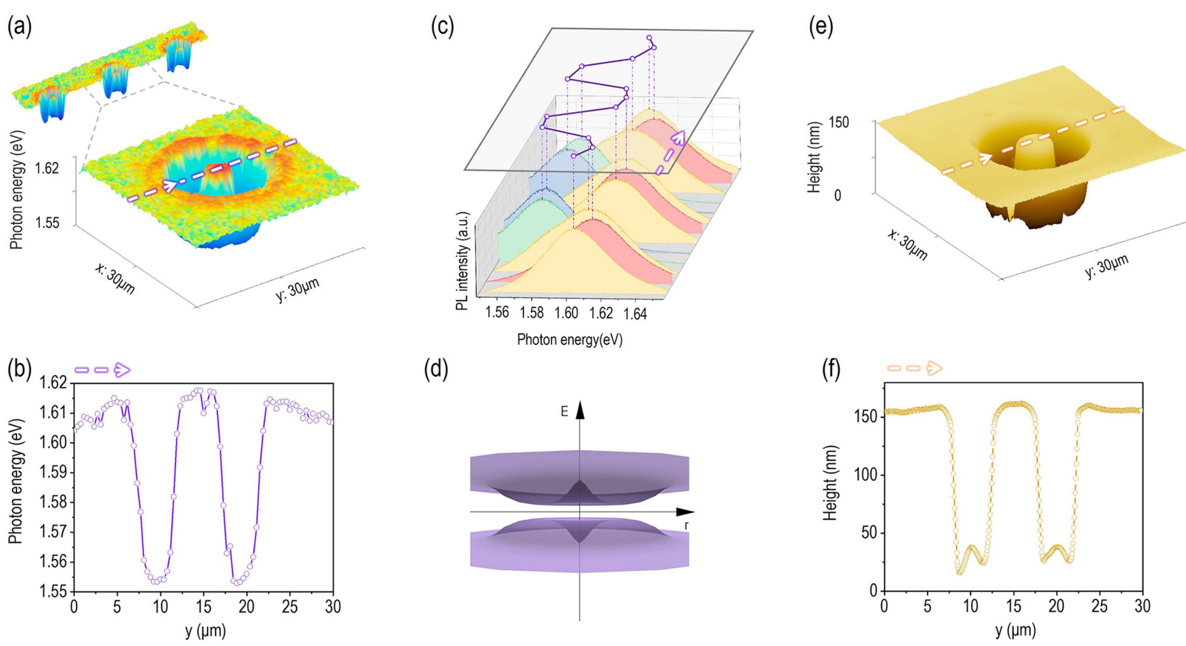

FIG. 3. Strain-induced spatial distribution of complex electronic structures in $MoSe_2$ monolayers. (a) A $30 \times 30\,\mu m$ PL peak mapping image of the strained pattern with Mexican hat deformation in a $MoSe_2$ monolayer. (b) The PL peak position profile of each Mexican hat along the white dashed lines in (a). (c) Schematic of the Mexican hat-type electronic structure. (d) The waterfall plot of PL peak spectra crossing the deformation profile along the white dashed lines in (a). (e) The AFM topography image of a $MoSe_2$ Mexican hat. (f) The height profile of the $MoSe_2$ Mexican cross section along the white dashed line in (e).

Published under an exclusive license by AIP Publishing

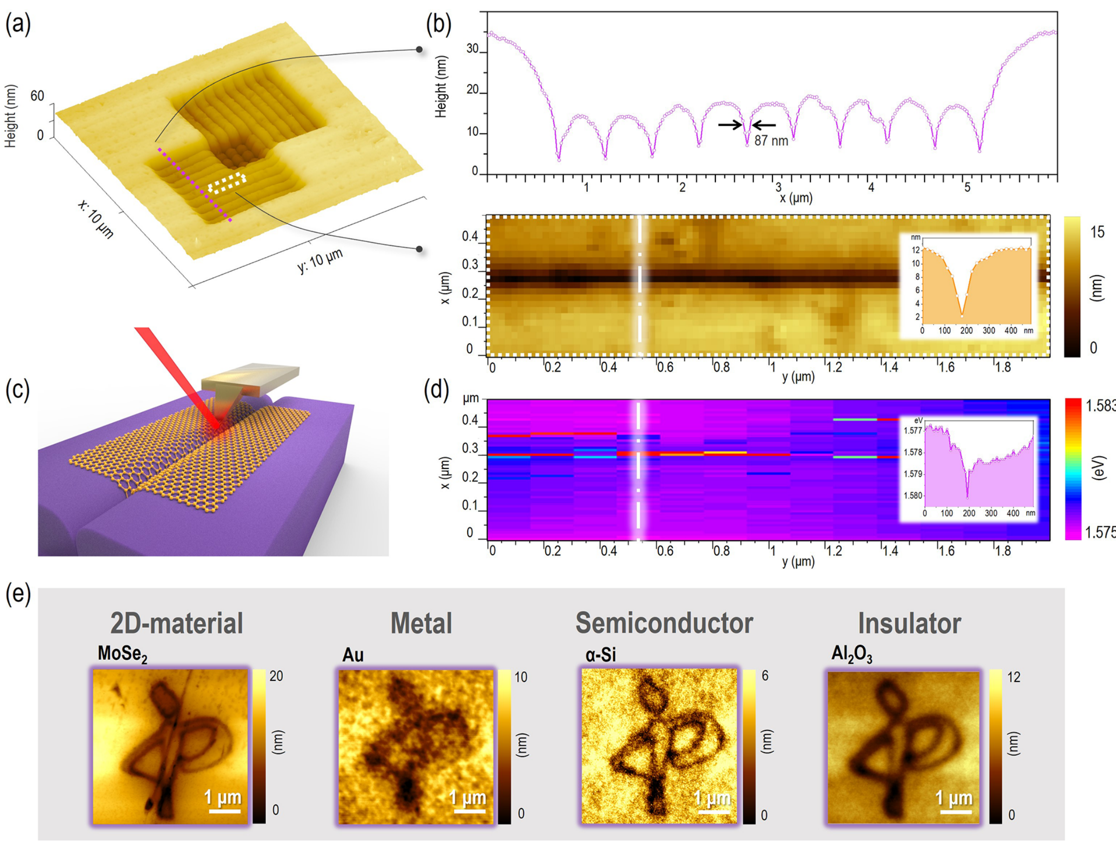

FIG. 4. Nano-strain lithography and strain patterning in other thin films. (a) A $10 \times 10\,\mu$m AFM topography image of a set of nano-grooves in a $MoSe_2$ monolayer. (b) Top: the height profile of the $MoSe_2$ nano-grooves' cross section along the purple dashed line in (a) and the FWHM of each stripe is about 90 nm. Bottom: A $2 \times 0.5\,\mu$m amplified AFM topography image of the groove in the white dashed area of (a), and each pixel is 20 nm. Inset: cross section along long and short dashed lines. (c) Schematic illustration of tip-enhanced photoluminescence (TEPL) mapping of the strained $MoSe_2$ monolayer. (d) Scanning TEPL spectroscopic map plotting peaks of the strained $MoSe_2$ monolayer of the white dashed area in (a). The size of each pixel is 80×8.3 nm. Inset: cross section along long and short dashed line. (e) AFM images of the strained patterns in different thin films (including $MoSe_2$, Au, α-Si, and Al_2O_3) imprinted by the electron beam, displaying the logo of the institute of physics.

Finally, we find that this strain patterning method is also appropriate for strain construction in other types of materials such as Au, α-Si, and Al_2O_3 films. Figure 4(e) displays the AFM images of the logo patterned strains on $MoSe_2$ (monolayer), Au (40 nm), α-Si (20 nm), and Al_2O_3 (20 nm), showing the universality of our method for multiple materials.

In summary, based on the electron induced photoresist deformation, we presented a non-contact method for direct and precise strain patterning in 2DMs by electron irradiation. In this way, the tensile, compress, or complex strains can be precisely generated in 2DMs with controllable positions, shapes, and sizes. We demonstrated that the special and complex pattern of the strained 2DM is able to be designed for a desired spatial profile of electronic structures of materials and for exploring unique physical properties. Meanwhile, the arrays of patterned strains exhibit a good uniformity. Finally, we also explore and demonstrate the capability of this method for differential strain distribution construction in the nanoscale and the universality of materials. As reported in the former theoretical and experimental studies, applying strain with specific distributions is able to generate valley orbital magnetization of 2DMs due to the Berry curvature dipole,[56] which would contribute to the development of valleytronics based on 2DMs such as valley Hall transport. Our work offers a unique strain engineering approach for complex strain distribution generation that is beyond the conventional extrinsic mechanical methods, and it is promising in promoting the applications of 2DMs in extensive fields ranging from nanoelectromechanical systems, high-performance sensing, and nontraditional photovoltaics to quantum information science.

See the supplementary material for Figs. S1–S7 for the process of sample preparation, the process of PMMA degradation, Raman peak mapping images of $MoSe_2$ monolayers exposed with the increasing electron dose ranging from 10^2 to 10^4 μAs/cm^2, the statistical report of strain distribution in a $MoSe_2$ monolayer, the statistical report of strained physical shapes in a $MoSe_2$ monolayer, microscopic pictures of different strained patterns imprinted by strain lithography in $MoSe_2$ monolayers, PL peak mapping, and local PL spectra along the white dashed line.

This work was supported by the National Natural Science Foundation of China under Grant Nos. 61888102, 11974386, 62174179, 12074420, U21A20140, and 61905274; the National Key

Published under an exclusive license by AIP Publishing

Research and Development Program of China under Grant Nos. 2018YFA0703700 and 2021YFA1400700; the Beijing Municipal Science & Technology Commission, Administrative Commission of Zhongguancun Science Park under Grant No. Z211100004821009; the Strategic Priority Research Program of Chinese Academy of Sciences (CAS) under Grant Nos. XDB33000000 and XDB28000000; the Key Research Program of Frontier Sciences of CAS under Grant Nos. QYZDJ-SSWSLH042 and XDPB22; and the Project for Young Scientists in Basic Research of CAS under Grant No.YSBR021. This work is also supported by the Synergic Extreme Condition User Facility, China.

AUTHOR DECLARATIONS

Conflict of Interest

The authors have no conflicts to disclose.

Author Contributions

S.D., Y.G., and C.G conceived and designed the experiments. S.D. fabricated the samples and carried out the experiments. S.D. and Y.G. performed the data analysis. S.D. and X.H. performed strain simulation. Z.Z. and Y.Z. provided CVD-grown $MoSe_2$ monolayers. L.H. and Q.B. provided assistance for the AFM, Raman, and photoluminescence measurements. C.S., R.Z., H.Y., and J.L. provided assistance for the experiment of EBL. A.J. provided assistance for the experiment of focused ion beam. S.D., Y.G., and C.G. co-wrote the manuscript with the participation of all co-authors.

DATA AVAILABILITY

The data that support the findings of this study are available from the corresponding authors upon reasonable request.

REFERENCES

[1] J. Bardeen and W. Shockley, Phys. Rev. **80**(1), 72 (1950).
[2] S. E. Thompson, G. Sun, Y. S. Choi, and T. Nishida, IEEE Trans. Electron Devices **53**(5), 1010 (2006).
[3] Y. Sun, S. E. Thompson, and T. Nishida, J. Appl. Phys. **101**(10), 104503 (2007).
[4] S. Manzeli, D. Ovchinnikov, D. Pasquier, O. V. Yazyev, and A. Kis, Nat. Rev. Mater. **2**(8), 17033 (2017).
[5] S. Bertolazzi, J. Brivio, and A. Kis, ACS Nano **5**(12), 9703 (2011).
[6] G. Wang, A. Chernikov, M. M. Glazov, T. F. Heinz, X. Marie, T. Amand, and B. Urbaszek, Rev. Mod. Phys. **90**(2), 021001 (2018).
[7] T. Cao, G. Wang, W. Han, H. Ye, C. Zhu, J. Shi, Q. Niu, P. Tan, E. Wang, B. Liu, and J. Feng, Nat. Commun. **3**, 887 (2012).
[8] X. Xu, W. Yao, D. Xiao, and T. F. Heinz, Nat. Phys. **10**(5), 343 (2014).
[9] J. R. Schaibley, H. Yu, G. Clark, P. Rivera, J. S. Ross, K. L. Seyler, W. Yao, and X. Xu, Nat. Rev. Mater. **1**(11), 16055 (2016).
[10] J. Feng, X. Qian, C.-W. Huang, and J. Li, Nat. Photonics **6**(12), 866 (2012).
[11] A. Castellanos-Gomez, R. Roldan, E. Cappelluti, M. Buscema, F. Guinea, H. S. van der Zant, and G. A. Steele, Nano Lett. **13**(11), 5361 (2013).
[12] P. Jia, W. Chen, J. Qiao, M. Zhang, X. Zheng, Z. Xue, R. Liang, C. Tian, L. He, Z. Di, and X. Wang, Nat. Commun. **10**(1), 3127 (2019).
[13] C. Palacios-Berraquero, D. M. Kara, A. R. Montblanch, M. Barbone, P. Latawiec, D. Yoon, A. K. Ott, M. Loncar, A. C. Ferrari, and M. Atature, Nat. Commun. **8**, 15093 (2017).
[14] J. Lu, A. H. Neto, and K. P. Loh, Nat. Commun. **3**, 823 (2012).
[15] N. Levy, S. A. Burke, K. L. Meaker, M. Panlasigui, A. Zettl, F. Guinea, A. H. C. Neto, and M. F. Crommie, Science **329**(5991), 544 (2010).
[16] T. P. Darlington, C. Carmesin, M. Florian, E. Yanev, O. Ajayi, J. Ardelean, D. A. Rhodes, A. Ghiotto, A. Krayev, K. Watanabe, T. Taniguchi, J. W. Kysar, A. N. Pasupathy, J. C. Hone, F. Jahnke, N. J. Borys, and P. J. Schuck, Nat. Nanotechnol. **15**(10), 854 (2020).
[17] D. Lloyd, X. Liu, J. W. Christopher, L. Cantley, A. Wadehra, B. L. Kim, B. B. Goldberg, A. K. Swan, and J. S. Bunch, Nano Lett. **16**(9), 5836 (2016).
[18] M. Zeng, J. Liu, L. Zhou, R. G. Mendes, Y. Dong, M. Y. Zhang, Z. H. Cui, Z. Cai, Z. Zhang, D. Zhu, T. Yang, X. Li, J. Wang, L. Zhao, G. Chen, H. Jiang, M. H. Rummeli, H. Zhou, and L. Fu, Nat. Mater. **19**(5), 528 (2020).
[19] W. Wu, L. Wang, Y. Li, F. Zhang, L. Lin, S. Niu, D. Chenet, X. Zhang, Y. Hao, T. F. Heinz, J. Hone, and Z. L. Wang, Nature **514**(7523), 470 (2014).
[20] Y. Peng, M. Que, J. Tao, X. Wang, J. Lu, G. Hu, B. Wan, Q. Xu, and C. Pan, 2D Mater. **5**(4), 042003 (2018).
[21] K. Zhang, J. Zhai, and Z. L. Wang, 2D Mater. **5**(3), 035038 (2018).
[22] Y. Nan, D. Tan, J. Shao, M. Willatzen, and Z. L. Wang, ACS Energy Lett. **6**(6), 2313 (2021).
[23] O. Iff, D. Tedeschi, J. Martin-Sanchez, M. Moczala-Dusanowska, S. Tongay, K. Yumigeta, J. Taboada-Gutierrez, M. Savaresi, A. Rastelli, P. Alonso-Gonzalez, S. Hofling, R. Trotta, and C. Schneider, Nano Lett. **19**(10), 6931 (2019).
[24] H. Kim, J. S. Moon, G. Noh, J. Lee, and J. H. Kim, Nano Lett. **19**(10), 7534 (2019).
[25] Y. Luo, N. Liu, X. Li, J. C. Hone, and S. Strauf, 2D Mater. **6**(3), 035017 (2019).
[26] H. Moon, E. Bersin, C. Chakraborty, A.-Y. Lu, G. Grosso, J. Kong, and D. Englund, ACS Photonics **7**(5), 1135 (2020).
[27] T. H. Ly, S. J. Yun, Q. H. Thi, and J. Zhao, ACS Nano **11**(7), 7534 (2017).
[28] H. Hattab, A. T. N'Diaye, D. Wall, C. Klein, G. Jnawali, J. Coraux, C. Busse, R. van Gastel, B. Poelsema, T. Michely, F. J. Meyer zu Heringdorf, and M. Horn-von Hoegen, Nano Lett. **12**(2), 678 (2012).
[29] A. Reserbat-Plantey, D. Kalita, Z. Han, L. Ferlazzo, S. Autier-Laurent, K. Komatsu, C. Li, R. Weil, A. Ralko, L. Marty, S. Gueron, N. Bendiab, H. Bouchiat, and V. Bouchiat, Nano Lett. **14**(9), 5044 (2014).
[30] Y. Zhang, M. Heiranian, B. Janicek, Z. Budrikis, S. Zapperi, P. Y. Huang, H. T. Johnson, N. R. Aluru, J. W. Lyding, and N. Mason, Nano Lett. **18**(3), 2098 (2018).
[31] H. Li, C. Tsai, A. L. Koh, L. Cai, A. W. Contryman, A. H. Fragapane, J. Zhao, H. S. Han, H. C. Manoharan, F. Abild-Pedersen, J. K. Norskov, and X. Zheng, Nat. Mater. **15**(3), 364 (2016).
[32] S. P. Koenig, N. G. Boddeti, M. L. Dunn, and J. S. Bunch, Nat. Nanotechnol. **6**(9), 543 (2011).
[33] T. M. G. Mohiuddin, A. Lombardo, R. R. Nair, A. Bonetti, G. Savini, R. Jalil, N. Bonini, D. M. Basko, C. Galiotis, N. Marzari, K. S. Novoselov, A. K. Geim, and A. C. Ferrari, Phys. Rev. B **79**(20), 205433 (2009).
[34] J. O. Island, A. Kuc, E. H. Diependaal, R. Bratschitsch, H. S. van der Zant, T. Heine, and A. Castellanos-Gomez, Nanoscale **8**(5), 2589 (2016).
[35] Z. Dai, L. Liu, and Z. Zhang, Adv. Mater. **31**(45), e1805417 (2019).
[36] S. Yang, C. Wang, H. Sahin, H. Chen, Y. Li, S. S. Li, A. Suslu, F. M. Peeters, Q. Liu, J. Li, and S. Tongay, Nano Lett. **15**(3), 1660 (2015).
[37] X. Liu, A. K. Sachan, S. T. Howell, A. Conde-Rubio, A. W. Knoll, G. Boero, R. Zenobi, and J. Brugger, Nano Lett. **20**(11), 8250 (2020).
[38] H. Zhang, F. Yang, J. Dong, L. Du, C. Wang, J. Zhang, C. F. Guo, and Q. Liu, Nat. Commun. **7**, 13743 (2016).
[39] C. F. Guo, V. Nayyar, Z. Zhang, Y. Chen, J. Miao, R. Huang, and Q. Liu, Adv. Mater. **24**(22), 3010 (2012).
[40] G. Brewer, *Electron-Beam Technology in Microelectronic Fabrication* (Elsevier Science, New York, 2012).
[41] H. Duan, J. Zhao, Y. Zhang, E. Xie, and L. Han, Nanotechnology **20**(13), 135306 (2009).
[42] Y. Koval, T. Borzenko, and S. Dubonos, J. Vac. Sci. Technol. B **21**(5), 2217 (2003).
[43] W. Chen and H. Ahmed, Appl. Phys. Lett. **62**(13), 1499 (1993).
[44] C. P. Ennis and R. I. Kaiser, Phys. Chem. Chem. Phys. **12**(45), 14902 (2010).
[45] I. R. Lewis and H. Edwards, *Handbook of Raman Spectroscopy: From the Research Laboratory to the Process Line* (CRC Press, New York, 2001).
[46] Z. Peng, X. Chen, Y. Fan, D. J. Srolovitz, and D. Lei, Light Sci. Appl. **9**(1), 190 (2020).
[47] W. Shi, M.-L. Lin, Q.-H. Tan, X.-F. Qiao, J. Zhang, and P.-H. Tan, 2D Mater. **3**(2), 025016 (2016).

Published under an exclusive license by AIP Publishing

[48]S. Horzum, H. Sahin, S. Cahangirov, P. Cudazzo, A. Rubio, T. Serin, and F. M. Peeters, Phys. Rev. B **87**(12), 125415 (2013).
[49]I. Bilgin, A. S. Raeliarijaona, M. C. Lucking, S. C. Hodge, A. D. Mohite, A. de Luna Bugallo, H. Terrones, and S. Kar, ACS Nano **12**(1), 740 (2018).
[50]H. P. Komsa, J. Kotakoski, S. Kurasch, O. Lehtinen, U. Kaiser, and A. V. Krasheninnikov, Phys. Rev. Lett. **109**(3), 035503 (2012).
[51]W. M. Parkin, A. Balan, L. Liang, P. M. Das, M. Lamparski, C. H. Naylor, J. A. Rodriguez-Manzo, A. T. Johnson, V. Meunier, and M. Drndic, ACS Nano **10**(4), 4134 (2016).
[52]X. Cheng, L. Jiang, Y. Li, H. Zhang, C. Hu, S. Xie, M. Liu, and Z. Qi, Appl. Surf. Sci. **521**, 146398 (2020).
[53]R. Frisenda, M. Drüppel, R. Schmidt, S. Michaelis de Vasconcellos, D. Perez de Lara, R. Bratschitsch, M. Rohlfing, and A. Castellanos-Gomez, npj 2D Mater. Appl. **1**(1), 10 (2017).
[54]J. Stadler, T. Schmid, and R. Zenobi, ACS Nano **5**(10), 8442 (2011).
[55]M. Rahaman, R. D. Rodriguez, G. Plechinger, S. Moras, C. Schuller, T. Korn, and D. R. T. Zahn, Nano Lett. **17**(10), 6027 (2017).
[56]J. Son, K. H. Kim, Y. H. Ahn, H. W. Lee, and J. Lee, Phys. Rev. Lett. **123**(3), 036806 (2019).

Published under an exclusive license by AIP Publishing